Available online at www.sciencedirect.com
SCIENCE DIRECT®
Journal of volcanology and geothermal research
ELSEVIER
Journal of Volcanology and Geothermal Research 125 (2003) 271–289
www.elsevier.com/locate/jvolgeores

Multiscale fracturing as a key to forecasting volcanic eruptions

Christopher R.J. Kilburn *

Benfield Hazard Research Centre, Department of Earth Sciences, University College London, Gower Street, London WC1E 6BT, UK

Received 10 October 2002; accepted 7 April 2003

Abstract

Among volcanoes reawakening after long repose intervals, the final approach to eruption (~1–10 days) is usually characterised by accelerating rates of seismicity. The observed patterns are consistent with the slow extension of faults, which continue to grow until they connect a pre-existing array of subvertical fractures and so open a new pathway for magma to reach the surface. Rates of slow extension are here investigated assuming that gravitational loading and magma overpressure create a fluctuating stress field in the country rock. Fluctuations are due to the intermittent growth of small cracks that cannot be detected by monitoring instruments. The rate of detected events is then determined by the frequency with which the concentration of strain energy around the tips of macroscopic faults becomes large enough to permit fault extension. The model anticipates oscillations in seismic event rate about a mean trend that accelerates with time, and identifies the rate of increase in *peak* event rate as a key indicator of the approach to eruption. The results are consistent with earlier empirical analyses of seismic precursors and, applied to data before the andesitic eruptions of Mt Pinatubo, Philippines, in 1991, and of Soufriere Hills, Montserrat, in 1995, they suggest that, for such volcanoes, reliable forecasts of magmatic activity might eventually be feasible on the order of days before eruption.

Keywords: eruption forecasting; fracture mechanics; slow cracking; Boltzmann distribution

1. Introduction

Volcanic eruptions are normally preceded by measurable signs of growing unrest. Although a range of geochemical and geophysical precursors have been identified (McGuire et al., 1995; Scarpa and Tilling, 1996; Sigurdsson, 2000), the most evident are increases in seismicity and ground deformation, caused by magma distorting the crust as it pushes its way to the surface.

Although magma will naturally follow existing fractures through a volcano, only under the special conditions of persistent activity is it likely to find an open pathway to the surface. More frequently, a new pathway must be formed by fracturing. For a magma body to migrate, therefore, it must normally exert a stress large enough to propagate a new fracture and to open the fracture sufficiently wide to permit flow against its own rheological resistance. Rates of magma ascent

* Fax: +44 (20) 7387 1612.
E-mail address: c.kilburn@ucl.ac.uk (C.R.J. Kilburn).

0377-0273/03/$ – see front matter © 2003 Elsevier Science B.V. All rights reserved.
doi:10.1016/S0377-0273(03)00117-3

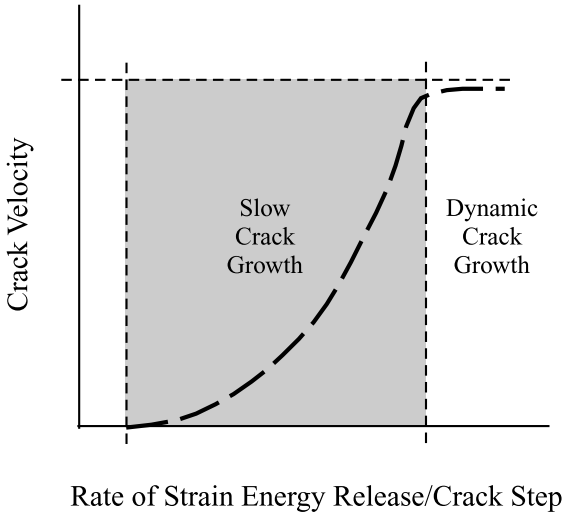

Fig. 1. Regimes in rates of crack growth. As a crack extends, it releases strain energy by relaxing surrounding rock, but consumes energy in creating and separating new crack surfaces. For large cracks, strain energy release dominates losses and the crack propagates dynamically. For cracks below a threshold size (determined by the fracture mechanical properties of rock and imposed stress field), the energy released is just greater than that consumed, so that the crack extends slowly under conditions of quasi-equilibrium (*shaded*). Conventional studies of dyke propagation assume that cracking is in the dynamic regime. This analysis focusses on cracking under quasi-equilibrium conditions. Note that, for step-like growth, crack velocity is proportional to event rate (see also Eq. 8; simplified after Main, 1991).

will thus be limited either by the rate of fracture growth, or by the rate of magma flow through the fracture.

Standard models of dyke propagation (Shaw, 1980; Spence and Turcotte, 1985; Lister, 1991) assume that fracturing is too fast to restrict magma ascent, so that the rate-limiting process is the ability of buoyant magma to overcome its viscosity. However, although rapid, dynamic failure is perhaps the most familiar form of fracturing, such behaviour is often preceded or replaced by a slower mechanism (Fig. 1), in which large fractures extend by the growth and coalescence of smaller cracks around their tips (Anderson and Grew, 1977; Heimpel and Olson, 1994; Main, 1999, 2000). Slow edifice fracturing, therefore, cannot be excluded as a control on rates of magma ascent. Indeed, given that standard models have yet to provide a basis for forecasting eruptions, it is pertinent to consider the case when slow edifice failure is the rate-limiting mechanism. This paper focusses on how populations of cracks interact to propagate a new pathway for magma to reach the surface. It will argue that similar styles of cracking can be expected over a large range of length scales and use this characteristic to propose a new procedure for forecasting eruptions from precursory accelerations in seismic event rate.

2. Empirical analyses of self-accelerating precursors

A slow-fracturing control is consistent with the characteristic of pre-eruptive signals that they show a restricted range of acceleration before an eruption, independent of the specific precursor in question. Voight (1988, 1989) quantified this range through an empirical power-law relation between the rate of change of a precursor ($\mathrm{d}\Omega/\mathrm{d}t$) and its acceleration ($\mathrm{d}^2\Omega/\mathrm{d}t^2$):

$$\mathrm{d}^2\Omega/\mathrm{d}t^2 = A(\mathrm{d}\Omega/\mathrm{d}t)^{\alpha} \quad (1)$$

where A is a constant and α lies between 1 and 2. Since an infinite $\mathrm{d}\Omega/\mathrm{d}t$ implies an uncontrolled rate of change, this condition is associated with the collapse of resistance to magma ascent and, as a result, with the start of an eruption. The forecasting potential of Eq. 1 is in describing the rate at which $\mathrm{d}\Omega/\mathrm{d}t$ approaches uncontrolled conditions.

Comparing precursory trends with the accelerations to failure recorded for engineering materials, Voight (1989) implicitly identified cracking as a probable control on pre-eruptive signals. This assumption was made explicitly in analyses of movements before dome explosions at Mount St Helens (McGuire and Kilburn, 1997) and of precursory seismicity before the 1995 eruption of Soufriere Hills volcano on Montserrat (Kilburn and Voight, 1998). These studies argued in particular that: (a) for a population of cracks, the exponent α in Eq. 1 increases from 1 to 2 as the dominant crack mechanism changes from crack nucleation to crack growth, and (b) since growth dominates the final stages of deformation, the ap-

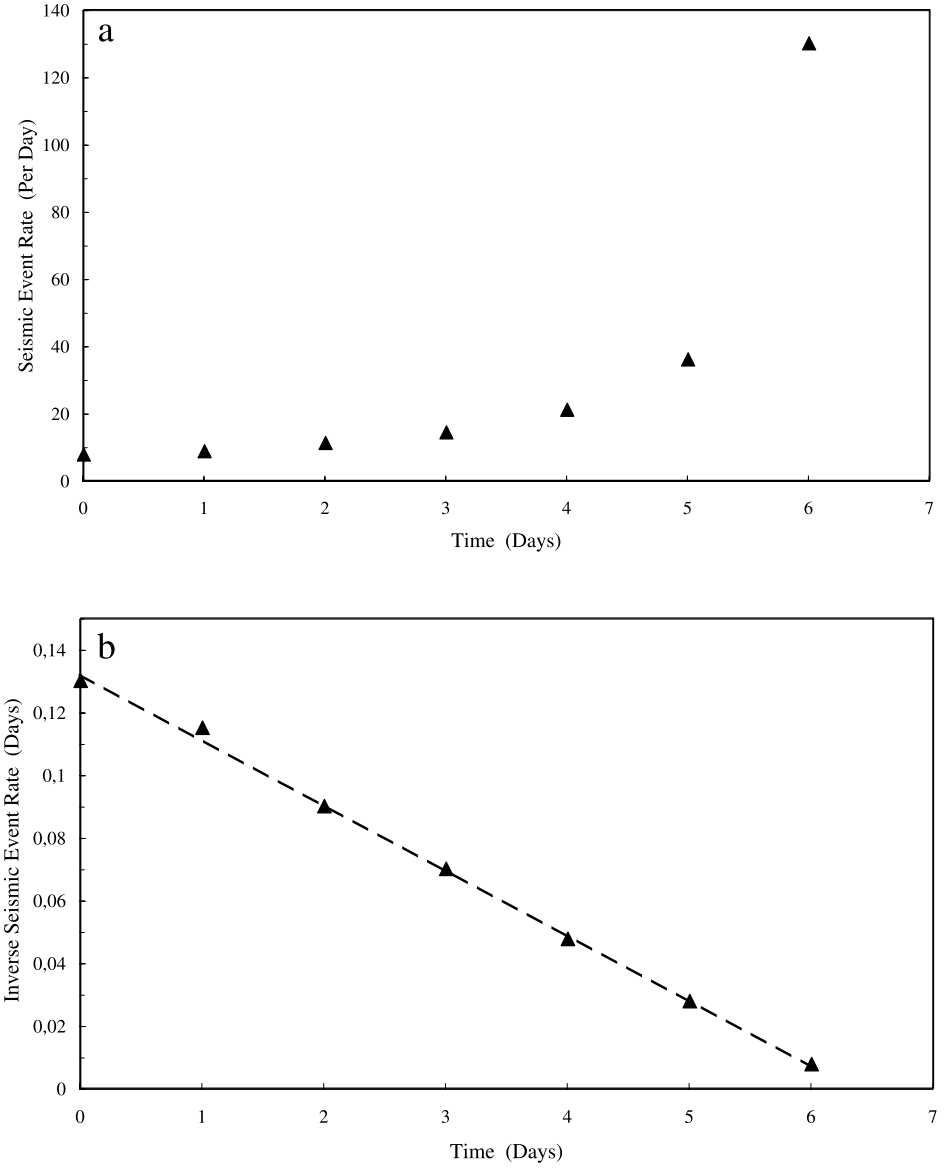

Fig. 2. Pre-eruptive conditions expected from Voight's empirical relation for $\alpha = 2$ (Eqs. 1 and 2. Although the change in event rate with time (panel a) may qualitatively appear to be exponential, it is in fact hyperbolic, so that the inverse rate shows a clear linear decrease with time (panel b).

proach to uncontrolled propagation is described by the condition $\alpha \approx 2$.

When $\alpha = 2$, Eq. 1 can be re-expressed in the form:

$$(\mathrm{d}\Omega/\mathrm{d}t)^{-1} = (\mathrm{d}\Omega/\mathrm{d}t)_0^{-1} - A(t - t_0) \quad (2)$$

where t is time, and $(\mathrm{d}\Omega/\mathrm{d}t)_0$ is the value of $(\mathrm{d}\Omega/\mathrm{d}t)$ when $t = t_0$. Thus, a plot of inverse rate against time follows a negative linear trend, so that the time at which the inverse rate is zero, corresponding to the uncontrolled condition when $\mathrm{d}\Omega/\mathrm{d}t$ tends to infinity, can be obtained by simple linear extrapolation of the measured trend to the time axis (Fig. 2). The linear form is important, be-

cause it is simpler to extrapolate than non-linear trends and so is less prone to observer error during an emergency.

The fracturing interpretation, however, was based on a comparison between Eq. 1 and a new relation for Ω derived from the growth of *microscopic* cracks (McGuire and Kilburn, 1997; Kilburn and Voight, 1998). The assumption that large-scale fracturing, which triggers measured seismic events, shows behaviour similar to microscopic cracking was justified retrospectively by the good agreement between expected and observed rates of seismicity. The assumption, however, has not been formally justified.

Eq. 1 has been applied to changes in precursory rates of seismic energy release, ground deformation and seismic event rate (Voight, 1988, 1989; Voight and Cornelius, 1991; Cornelius and Voight, 1995, 1996; McGuire and Kilburn, 1997; Kilburn and Voight, 1998; De la Cruz-Reyna and Reyes-Dávila, 2001; Reyes-Dávila and De la Cruz-Reyna, 2002). Of these, seismic event rate is the most useful during an emergency because it is simple to measure, even with a temporary monitoring network, and requires minimal data processing. Accordingly, this paper will focus on how seismic event rate can be related to the macroscopic development of crack populations and the propagation of a pathway that allows magma to breach the surface. By concentrating on the extension of a fracture system, the analysis is implicitly directed towards changes in the rate of volcano-tectonic (VT) events, rather than the long-period (LP) events that are commonly associated with pressure changes induced by fluids (e.g. magma, released magmatic volatiles or meteoric fluids) migrating through fractures (Chouet, 1996; McNutt, 2000).

3. Features of pre-eruptive seismicity

Short-term pre-eruptive seismicity normally evolves at depths of less than 5–7 km (McNutt, 1996). Events tend to cluster (a) beaneath the volcano's axis, within an approximately cylindrical region some 1–3 km across (Fig. 3) and, especially during the initial stages of unrest, also (b) around one or more locations with epicentres offset from the axis by several kilometres (Aspinall et al., 1998; De Natale et al., 1991; McNutt, 1996; Harlow et al., 1996). Although events of magnitude 5–6 have been recorded (Smith and Ryall, 1982; Savage and Cockerham, 1984), most have magnitudes less than 2 (Hill et al., 1990; McNutt, 1996). For magnitudes of 0–2, the events are associated with movements of about 1–10 mm over corresponding distances of 10–100 m (McNutt, 2000).

During the final acceleration to eruption, which evolves over intervals of $\sim$1–10 days and is often dominated by events within the 'seismic cylinder' beneath the volcano's axis, the total number of events with magnitudes of about 1 or more is frequently $\sim 10^2$–10^3 (Figs. 6 and 7). The implied cumulative displacement is thus $\sim$10 m or less. In comparison, magma bodies triggering the precursors have notional lengths of $\sim$1 km and must force their way at least through $\sim$1 km of a volcanic edifice. Apparently, the detected events cannot be explained by the simple upward displacement of a dyke. Indeed, events often occur throughout the whole axial seismic cylinder during the entire precursory sequence without a strongly preferred upward migration (Aspinall et al., 1998; Harlow et al., 1996). The simplest interpretation is that cracks grow throughout the whole axial seismic cylinder before they eventually join together an array of previously isolated fractures. Once connected, these fractures form the new pathway for magma ascent. Because the key objective of this paper is to investigate the use of accelerating seismicity for forecasting eruptions, the analysis concentrates on events triggered within the axial seismic cylinder (Fig. 3). The role of non-axial seismic clusters is left for evaluation elsewhere.

Precursory events are commonly dominated by reverse and strike-slip faulting. Such behaviour is consistent with slip movements under compressional stress (due to gravitational loading and to magmatic overpressure) in rock surrounding an array of subvertical fractures (Fig. 3). Thus, even in a compressional field, subvertical fractures can be preferentially reactivated when compression is smaller horizontally than vertically, while

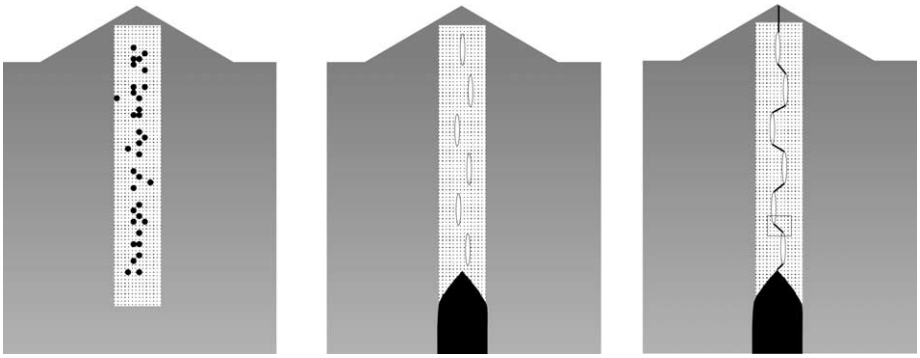

Fig. 3. (Left) Pre-eruptive seismicity is commonly concentrated within an approximately cylindrical region around a volcano's axis between a magma body and the surface (especially during the final approach to eruption; see text). Events occur throughout the 'seismic cylinder' for the entire pre-eruptive crisis; an upward migration of events is not usually obvious. Such behaviour is interpreted (centre and right) in terms of the extension of, and movements along, faults connecting pre-existing subvertical fractures above the magma body (black). The characteristic length L of the connection between vertical fractures (e.g. small box, right) is $\sim$10–100 m. See Fig. 4 for details of fault extension. As discussed in the text, additional seismicity may occur in clusters with epicentres offset from the volcano's axis, but this is not incorporated in the present analysis. (Not to scale.)

slip movements are favoured by the net uplift of country rock between a magma body and the surface. Seismic events are triggered as the country rock slips within restricted volumes, each with a characteristic dimension L (notionally 10–100 m) between the subvertical fractures (Fig. 3). The restricted volumes may contain either (a) a collection of smaller fractures that eventually coalesce into a new fault, or (b) a continuous fault that slips after small fractures have grown and coalesced around its ends. In either case, displacement along the length L, which triggers a detectable seismic event, is determined by the growth of the small cracks. With repeated cycles of fracture extension and slip, faults within the restricted volumes eventually link with the subvertical fractures to create a major new pathway to the surface.

4. Time-dependent rock fracture

Repeated failure can occur under constant applied stress. Also called static fatigue, such a style of failure is a well-known property of composite materials, as well as rock (Anderson and Grew, 1977). It is encouraged by high temperatures, which elevate the rate of chemical interactions with a circulating fluid, especially water, and also increase pore pressures in the host rock, thereby further reducing frictional resistance along existing faults.

Fractures remain stable until subjected to a stress large enough to overcome sliding friction and to provide the energy for opening new crack surfaces (Scholz, 1990). Although not important at very small scales, friction is the dominant factor stabilising macroscopic fractures. Expressed energetically, when failure occurs the strain energy E_m supplied by intruding magma is absorbed by deforming the country rock (Scholz, 1990):

$$E_m = E_d + E_f + E_{nc} + E_s \quad (3)$$

where E_d is the energy used for ground uplift, E_f is the frictional energy lost in sliding along fractures, E_{nc} is the energy required for creating new crack surfaces, and E_s is the radiated seismic energy.

Typically, E_{nc} is much smaller than the other terms on the right-hand side of Eq. 3 and so is usually neglected in deformation and seismic studies. However, whereas E_d, E_f and E_s are associated with instantaneous responses to magma intrusion, E_{nc} is inherently time-dependent. Moreover, since new crack surfaces must be formed before an existing fault can be displaced (thereby affecting all the other energy terms), E_{nc} emerges as a small but essential control on rates of crustal deformation and seismicity. The present analysis

therefore focusses on how energy is supplied for creating new crack surfaces and for controlling observed rates of seismicity.

5. Seismic event rates and stress fluctuations

Detected seismic events are produced as faults grow between the ends of widening, subvertical fractures (Fig. 3). Fault extension itself is controlled by processes operating within the zone of stress concentration, or *process zone*, that develops around the fault's tip when it is put under stress (Atkinson, 1984; Main, 1991; Main and Meredith, 1991; Lockner, 1993; Cowie and Shipton, 1998). Within this zone, arrays of smaller, tensile cracks and slip surfaces grow and coalesce until the whole zone is broken, so extending the parent fault (Fig. 4). However, just as a large fault grows by the extension and coalescence of small cracks around its tips, so each of the small cracks also grows by the extension and coalescence of the next smaller population of cracks in its own process zone. Fracturing is thus viewed as a multiscale process, major fractures being the result of cracking at successively smaller scales, down to the submicroscopic dimensions at which cracks nucleate. Excluding nucleation events, therefore, it should be possible to resolve a recorded event into a sequence of growth steps among smaller cracks whatever the scale of observation (Fig. 4).

As a crack of any size extends, it releases energy by relaxing the strain in the rock immediately around its new extension, but consumes energy in creating and separating the new crack surfaces (e.g. Lawn, 1993). Extension continues as long as the energy released exceeds the amount consumed. Among a population of cracks, however, the overall pattern of growth is complicated by interference between neighbouring cracks. Thus, the zone of stress concentration around a crack tip is enclosed by regions of reduced stress (Cowie, 1998). Accordingly, the growth of one crack can be stalled if it extends into the zone of reduced stress (or stress shadow) from a neighbouring crack. The first crack may then be reactivated as the local stresses change to a more favourable distribution, in response to the extension of another neighbour.

Slow cracking is thus characterised also by fluctuating stresses in the process zones of cracks of all sizes. Events due to cracks smaller than a threshold value (determined by observing conditions, such as instrument sensitivity, the size and

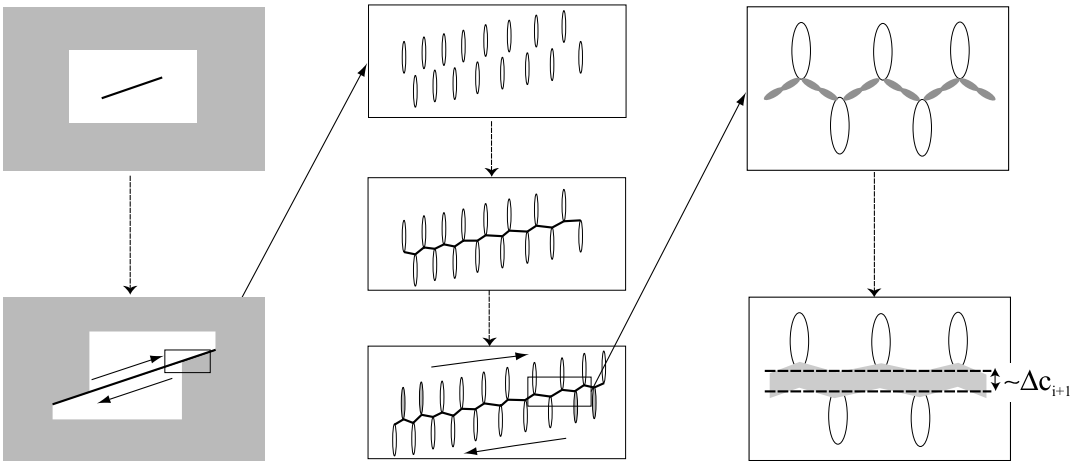

Fig. 4. Faults extend by activating existing cracks in the process zones around their tips. Even if in absolute compression, the horizontal component is smaller than the vertical component, yielding a tensile *differential* horizontal stress. Hence tensile cracks open, extend and coalesce around the tips of the fault. Upon coalescence, the fault can move along its new extension (left and centre). (Right) The separation between new crack surfaces is controlled by relaxation of stress in previously unbroken rock (shaded), which is on the order of the extension rather than the length of the existing cracks (white) in the process zone. Note that the figures are scale-independent.

geometry of the monitoring array, the depth of fracturing, and the attenuating properties of the fracturing medium) cannot be distinguished individually but, instead, they control the frequency of the background variation in stress. The number of events detected seismically then depends on the rate at which the background stress is locally high enough to extend fractures that are larger than the threshold value.

5.1. Quantifying rates of cracking

Assuming that stress fluctuations occur randomly in a volume under stress, the probability of crack propagation is given by the proportion of cracks that have the required additional strain energy around their tips at any particular moment. If the volume consists of ϕ *potential* controlling cracks (where ϕ is large), then the number of ways Θ that random energy fluctuations will yield m_i *active* cracks, with the strain energy ε_i necessary for propagation, is:

$$\Theta = \emptyset! / \prod_i m_i! \tag{4}$$

Importantly, it is not necessary to specify which particular members of the crack population are active at any given moment, but only the number m_i that are active. The problem thus becomes analogous to the classical Boltzmann analysis in statistical physics of describing the energy distribution among a large population of randomly moving gas molecules (and, hence, of deriving the associated gas pressure) for which it is important to know the total number of molecules in a particular energy state, rather than to follow the changes in energy state of individual molecules (Ruhla, 1992). Following the Boltzmann analysis (Ruhla, 1992; Landau and Lifshitz, 1999), therefore, the probability $P(\varepsilon_i)$ that a crack tip is supplied with the extra energy ε_i is given by determining the maximum value of Θ, which corresponds to the state of statistical equilibrium:

$$P(\varepsilon_i) = \frac{[\text{Number of ways of containing energy } \varepsilon_i]}{[\text{Total number of energy states available}]}$$

$$= (1/Z)e^{-\varepsilon_i/nRT} \tag{5}$$

where the total internal energy nRT consists of the ideal gas constant, R (8.314 J mol^{-1} K^{-1}), absolute temperature, T, and the number of moles n of rock involved in cracking a process zone; although originally determined from gas thermodynamics, the use of R is valid also for the internal energy of solids. The partition function $Z = \Sigma_i e^{-\varepsilon_i/nRT}$ measures the total number of energy states in which a crack tip could exist.

The probability of cracking in Eq. 5 can be transformed into expected rates of cracking, by introducing the mean frequency f of stress fluctuations, so that $dN(t)/dt$, the expected crack rate (or rate of successful stress fluctuations for crack extension), becomes $fP(\varepsilon_i)$. Given that f and Z are constant for a given system, it follows that:

$$dN(t)/dt = f^* e^{-\varepsilon i/nRT} \tag{6}$$

where $f^* = f/Z$.

Eq. 6 combines cracking at different scales through the exponent and pre-exponential term on its right-hand side. Thus, while f^* describes the rate of stress fluctuations (involving those due to cracking at sizes too small to be resolved), the term $e^{-\varepsilon_i/nRT}$ describes the proportion of those fluctuations that provide the energy ε_i for activating the cracks that can be detected. Importantly, no constraints have been imposed on *absolute* crack size, so that the form of Eq. 6 should be valid for rates of cracking at all scales (although some limits will be introduced later).

Eq. 6 provides a second link between fracturing at different scales, by noting that each event N corresponds both (a) to a growth step for one member of a population of fractures of a particular size (at, say, Scale 1), and (b) to a cycle of growth and coalescence among the smaller cracks (Scale 2) in the process zone of the Scale-1 fracture (Fig. 4). Coalescence terminates the acceleration in Scale-2 event rate and so coincides with the peak rate achieved by the Scale-2 cracks (Fig. 5). Accordingly, a Scale-1 growth step can be expressed in terms of the peak rate of Scale-2 cracking by:

$$dN_1/dt = \Psi dN_{2P}/dt \tag{7}$$

where, to simplify notation, $N(t)$ is replaced by N and understood to be a function of time, the subscripts 1 and 2 denote the scale of cracking, sub-

script P denotes peak value, and Ψ is the scaling factor ($\Psi < 1$). This relation will be used later to relate detected seismicity to fracturing at different scales.

By utilising the Boltzmann distribution in Eq. 5, the derivation of Eq. 6 assumes an equilibrium size–frequency distribution for the values of background energy ε_i, smaller values having a greater frequency of occurrence. For the event rate to accelerate, therefore, the preferred value of ε_i for further cracking must decrease with time (such that the associated frequency of occurrence increases). The next section describes how such a condition occurs naturally as propagating fractures release the strain energy already stored in the host rock.

5.2. Event rate and rate of crack growth

Persistent slow cracking is maintained while the rate of energy released by crack growth just exceeds that required for new cracks to form. From standard theory, this quasi-equilibrium condition can be related to the total change in energy ε_i in Eq. 6 by (e.g. Griffith, 1920; Jaeger, 1969; Scholz, 1990; Lawn, 1993):

$$\varepsilon_i = \varepsilon_{NS} - \varepsilon_G \tag{8}$$

where ε_{NS} is the energy required to create new fracture surfaces, and ε_G is the excess strain energy released by the surrounding rock as a crack grows (equivalent to the total strain energy minus the energy required to move new crack surfaces apart). In terms of *differential* applied stress S and material properties (Jaeger, 1969; Scholz, 1990; Lawn, 1993):

$$\varepsilon_i = 2\alpha w\Delta c - B(S^2/Y')cw\Delta c \tag{9}$$

where α is the energy per unit area to create new surfaces, w and c are the width and length of the extending crack, and Δc is the increase in length per crack step. The constant B describes the geometry of loading, and for straight-edged fractures is $\sim\pi$, while the effective Young's modulus Y' is a function of the actual modulus Y and Poisson's ratio ν_p (about 0.3 for crustal rock), the form of which depends on deformation conditions (e.g. for plane stress, $Y' = Y$, whereas for plane strain, $Y' = Y/(1-\nu_p^2)$ (Lawn, 1993); to a first approximation, $Y' \sim Y$). Crack width (i.e. the length of its propagating edge), α and Y' are assumed to be constant.

The prevailing stress field appears in the second term on the right-hand side of Eq. 9. Importantly, this term incorporates only the magnitude of S and so has the same form for compressional and tensile fields, as well as for different modes of rock failure (Scholz, 1990; Lawn, 1993).

For a single crack:

$$c = c_0 + N\Delta c \tag{10}$$

where c_0 is the initial crack length, Δc is the increase in length per crack step (assumed constant), and N is the number of steps already taken in extending from c_0.

Eqs. 8–10 can be combined to relate the energy for crack extension to initial crack size and to the previous amount of cracking:

$$\varepsilon_i/nRT = \eta - \gamma(c_0/\Delta c) - \gamma N \tag{11}$$

where $\eta = 2\alpha w\Delta c/nRT$ (the ratio [Surface energy consumed in extending crack by Δc]/[Total internal energy]) and $\gamma = B(S^2/Y')w\Delta c^2/nRT$ (the ratio [Strain energy released in extending crack by Δc]/[Total internal energy]). As expected from the previous section, as N increases with continued fracturing, so the extra energy ε_i for crack extension decreases. Moreover, the fact that the change in ε_i depends on the number of incremental increases in length also demonstrates how the total energy in the fracture system can be viewed in terms of the net release of *packets* of energy, each packet associated with a crack extension of Δc.

Eq. 11 has been developed for the growth of a single crack. A similar type of relation is anticipated for a population of cracks, replacing values of w and c_0 for a single crack with those averaged over the whole population, especially if the crack lengths follow a fractal frequency distribution (Main, 1991). Accordingly, it is assumed that Eq. 11 is valid for a collection of cracks using average values for initial crack dimensions. Eq. 11 can then be substituted for ε_i in Eq. 6 to yield for the event rate:

$$dN/dt = f^* e^{-\eta} e^{\gamma c_0/\Delta c} e^{\gamma N} \tag{12}$$

recalling that N is a function of time ($N(t)$).

According to Eq. 12, event rates during crack growth are expected to increase exponentially with the total number of growth steps N already completed. Such an exponential dependence is important because relations of the form $d\omega/dt \propto e^{K\omega}$ (where K is a constant and ω is the relevant event number) yield $d^2\omega/dt^2 \propto e^{K\omega} d\omega/dt \propto (d\omega/dt)^2$, identical to Voight's empirical relation (Eq. 1) with $\alpha = 2$. Indeed, after manipulation (Appendix), Eq. 12 can be re-expressed in the same form as Eq. 2:

$$(dN/dt)^{-1} = (dN/dt)_0^{-1} - \gamma(t - t_0) \quad (13)$$

$(dN/dt)_0$ is the value of dN/dt when $t = t_0$. Eqs. 12 and 13 thus provide a direct link between macroscopic rock fracture and the Voight model.

5.3. Detected seismicity and the opening of magmatic pathways

Applied to volcanic precursors, the detected event rate immediately before an eruption is attributed to the frequency of growth steps along faults in the axial seismic cylinder under stress (Fig. 3). This rate accelerates with time until at least one fault has coalesced with a subvertical fracture. At this stage, some of the excess strain energy for new cracking is dissipated, because the fault has propagated into the void of an open fracture, rather than into country rock. The open fracture thus extends by the length of the newly coalesced fault. Under the maintained magmatic stress, however, cracking continues as other faults and fractures grow in the seismic cylinder. Against an accelerating overall trend, therefore, the variation of event rate with time (Fig. 5) is expected to show episodes of acceleration (fault extension and coalescence) separated by intervals of reduced event rate (energy dissipation at coalescence).

While detected events correspond to growth steps along faults, the local peak values correspond to growth steps among the subvertical fractures. The two cases are related to cracking at different scales: faults extend by the coalescence of cracks in their process zones, whereas subvertical fractures extend by opening newly coalesced faults. Accordingly, each sequence of accelerating event rate and the change in peak value from one sequence to the next are both expected to increase according to trends of the form of Eq. 12. Thus, setting the detected seismicity (fault steps) as Scale-2 events and their peak values (main-fracture steps) as Scale-1 events, Eqs. 7 and 12 lead to:

$$dN_2/dt = f_2^* e^{-\eta_2} e^{\gamma_2 c_{02}/\Delta c_2} e^{\gamma_2 N_2} \quad (14a)$$

$$(dN_2/dt)^{-1} = (dN_2/dt)_0^{-1} - \gamma_2(t - t_0) \quad (14b)$$

and

$$dN_{2P}/dt = (1/\Psi) dN_1/dt = (f_1^*/\Psi) e^{-\eta_1} e^{\gamma_1 c_{01}/\Delta c_1} e^{\gamma_1 \Psi N_{2P}} \quad (15a)$$

$$(dN_{2P}/dt)^{-1} = (dN_{2P}/dt)_0^{-1} - \Psi\gamma_1(t - t_0) \quad (15b)$$

noting, from Eq. 7, that $N_1 = \Psi N_{2P}$.

Given that the variation with time in peak event rate describes the extension of the primary subvertical fractures, it follows that Eq. 15 is the more appropriate for monitoring the growth of a new magmatic pathway. Hence, in contrast to changes in actual event rate, as used in previous studies (e.g. Cornelius and Voight, 1996; Kilburn and Voight, 1998), the change in peak event rate may be the more reliable trend for forecasting the time of an eruption.

5.4. Submicroscopic limits

Although no macroscopic constraints have been placed on Eq. 12, a submicroscopic limit can be perceived when growing cracks are the equivalent of crack nuclei. By definition, such nuclei are the smallest cracks available, so that the extension of their process zones must depend on mechanisms other than the growth of even smaller cracks. In this limit, rates of crack growth are controlled by molecular processes, of which the most favoured is chemically enhanced stress corrosion (Charles and Hillig, 1962; Wiederhorn and Bolz, 1970; Lockner, 1993). Such corrosion assumes that fluids chemically weaken molecular bonds in a ma-

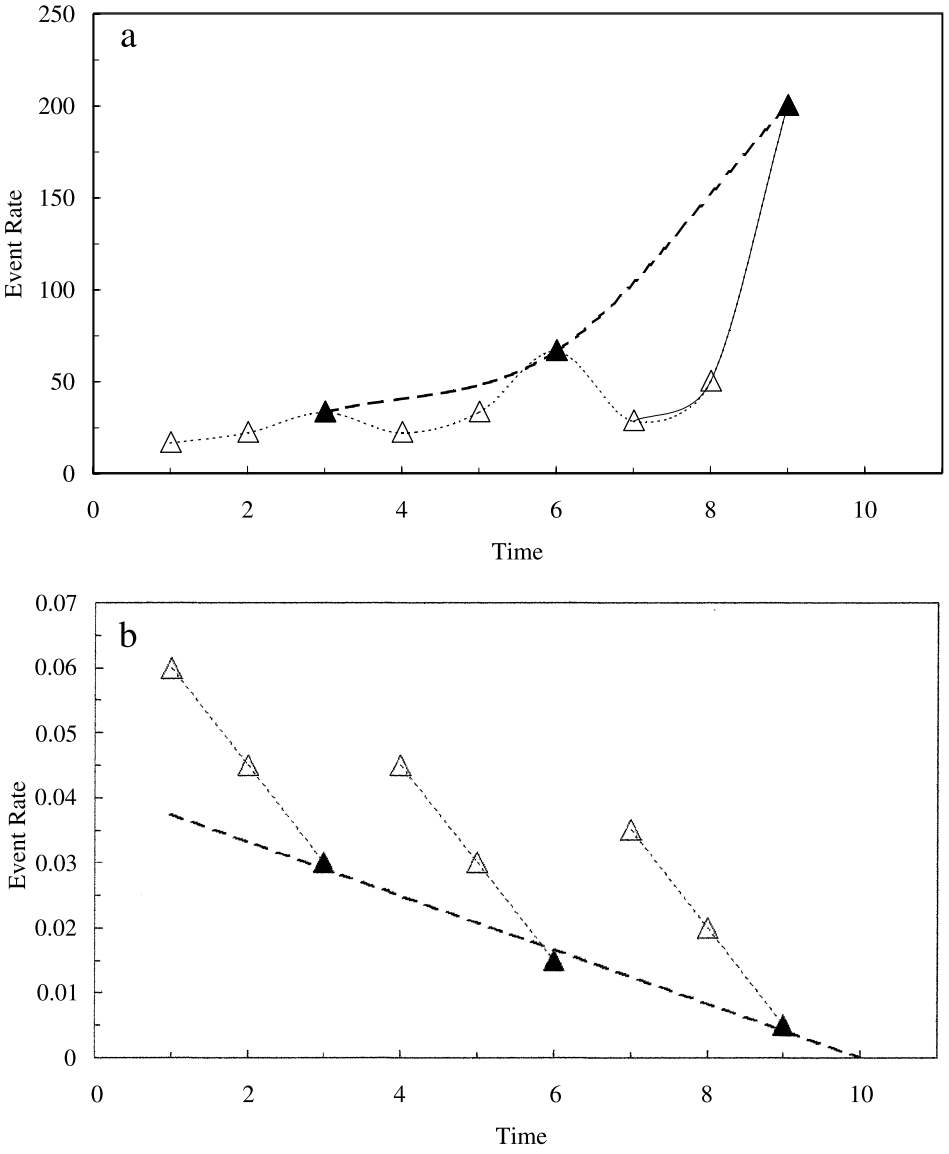

Fig. 5. Schematic change in peak event rate as precursory trend before an eruption. (a) The recorded event rate (all triangles) increases with time about an oscillating trend (small dashes). Plotted on an inverse-rate diagram (panel b), however, different linear inverse trends become apparent between sequences of cracks coalescing aound the tips of faults (open triangles with small dashed lines) and in the extension of the faults themselves, given by the peaks in monitored event rate (filled triangles with large dashed line).

terial, so promoting the growth of crack nuclei when an external stress is applied. The chemical reactions require repeated attempts by excited molecules to break the bonds around a crack tip. The rate of crack growth thus depends on the mean frequency ν of molecular attempts to break bonds and on the probability $P(E_i)$ that an attempt will have sufficient energy E_i for breakage to occur. Replacing the background rate of stress fluctuation f with ν and the proba-

bility $P(\varepsilon_i)$ with $P(E_i)$, analogy with the development of Eq. 6 yields for the frequency of crack events:

$$dN/dt = (\nu/Z)e^{-E_i/nRT} \quad (16)$$

where n is now the number of moles involved in the chemical reactions that cause a crack to extend, and Z is the appropriate partition coefficient.

As with ε_i in Eq. 6, E_i decreases linearly with the excess energy released by previous crack events, such that $E = E^* - E_G$, where E^* is the activation energy for a chemical reaction to occur and $E_G \propto (c_0 + N\Delta c)$ is the energy available from the N previous crack events. Accordingly, using the same arguments as for Eqs. 6 and 12, Eq. 16 again leads to a result of the form $d\omega/dt \propto e^{K\omega}$, identical to that of Eqs. 14 and 15. Although the controlling factors differ, therefore, the crack growth law at the smallest scale is expected to have the same form as that at larger scales, thus accounting for the previous success in extrapolating submicroscopic crack models to macroscopic conditions (McGuire and Kilburn, 1997; Kilburn and Voight, 1998).

6. Application to eruption precursors

For initial verification of the slow-cracking model, Eqs. 14 and 15 have been tested against the seismic precursors recorded before the eruptions of Soufriere Hills on Montserrat in 1995 and of Pinatubo, in the Philippines, in 1991. In both cases, the eruptions began with the extrusion of andesitic lava domes. However, whereas Pinatubo's activity evolved within days into a plinian eruption (Newhall and Punongbayan, 1996), activity at Soufriere Hills has continued to 2003 (the time of writing) to be dominated by dome growth with minor explosivity (Young et al., 1998). Accordingly, precursory data from the two eruptions may cover the spectrum of behaviour expected at least from andesitic volcanoes.

6.1. Soufriere Hills, Montserrat, 1995

During the 2 weeks before magma breached the surface on 15 November 1995, after a repose interval of some 350 years, precursory activity at Soufriere Hills was characterised by a 10-fold increase in the rate of earthquake occurrence (Kilburn and Voight, 1998). Recorded by an array of short-period, vertical-component seismometers (Aspinall et al., 1998), most events appear to have had magnitudes of less than 2.5, although some achieved magnitude 4 (Power et al., 1998).

The recorded seismic event rates and their inverse are shown in Fig. 6. Kilburn and Voight (1998) analysed these trends using a slow-fracture model extrapolated from conditions for microscopic cracking. They identified a mean linear trend among the inverse-rate data, but, owing to the scatter, speculated that the event rates might have been controlled by the growth of more than one fracture system. Their analysis, however, did not account for the possibility – highlighted by the present analysis – that accelerating fracture propagation may be recorded as a sequence of increasing *peaks* in seismic event rate. Indeed, when the variations in peak rate (dN_P/dt) are analysed using the sequence of minimum values on the inverse-rate plot, a clear negative linear trend emerges with time (Fig. 6), described by:

$$(dN_P/dt)^{-1} = 0.037 - 0.0024t \quad (17)$$

with an r^2 regression coefficient of 0.99 (for dN_P/dt in events per day and t in days; see Kilburn and Voight (1998) for an error analysis). At the same time, event-rate sequences between peaks show negative linear inverse rates with gradients of about 0.01 (estimated by eye from Fig. 6).

The inverse-rate trend in earthquake occurrence is thus consistent with the present model, for which peak seismic event rate is the key factor for monitoring the rate of fracture growth. The high-value data on the inverse-rate trend can then be attributed not to scatter, but to lower event rates between sequences of accelerating seismicity. Importantly, had this interpretation been available at the time, a linear negative trend among inverse-rate minima could have been identified at least by 09 November. The four minima between 02 and 09 November yield the regression line $(dN/dt)^{-1} = 0.031 - 0.0019t$ ($r^2 = 0.99$) and an expected eruption date of 16 November, 1 day

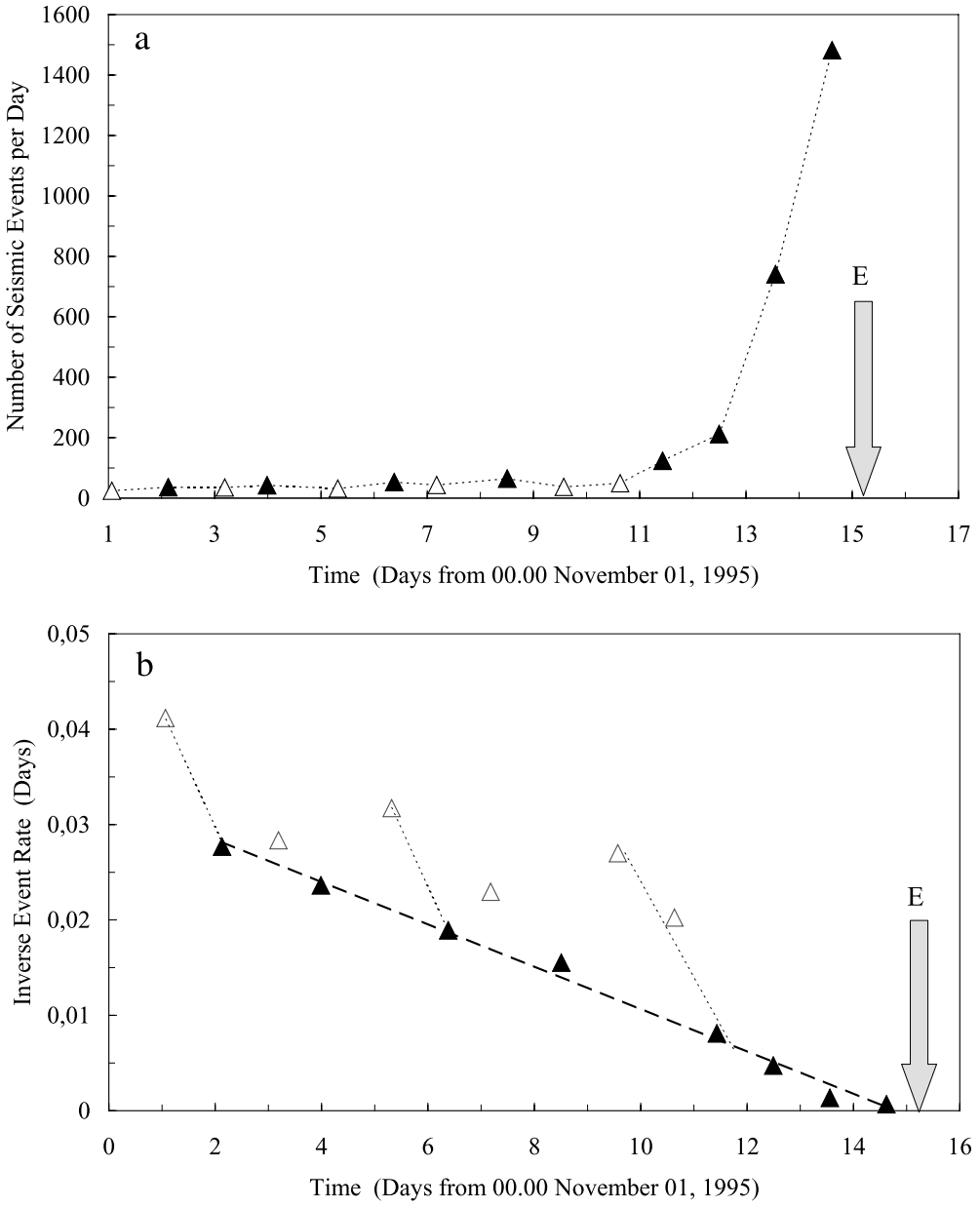

Fig. 6. (a) Change in recorded seismicity before the 1995 eruption of Soufriere Hills on Montserrat. Filled and open triangles correpond to symbols used in panel b. Arrow E marks onset of magmatic activity. On an inverse-rate diagram (panel b), the filled triangles, which correspond to inverse-rate minima, lie along a linear trend (large dashed line). Such a trend might have been recognised by Day 8–9 and so have provided a maximum 6-day warning of eruption. Note that peak values are more readily identified from the inverse-rate minima than the actual event-rate maxima, and that steeper linear trends occur among individual sequences (small dashed lines).

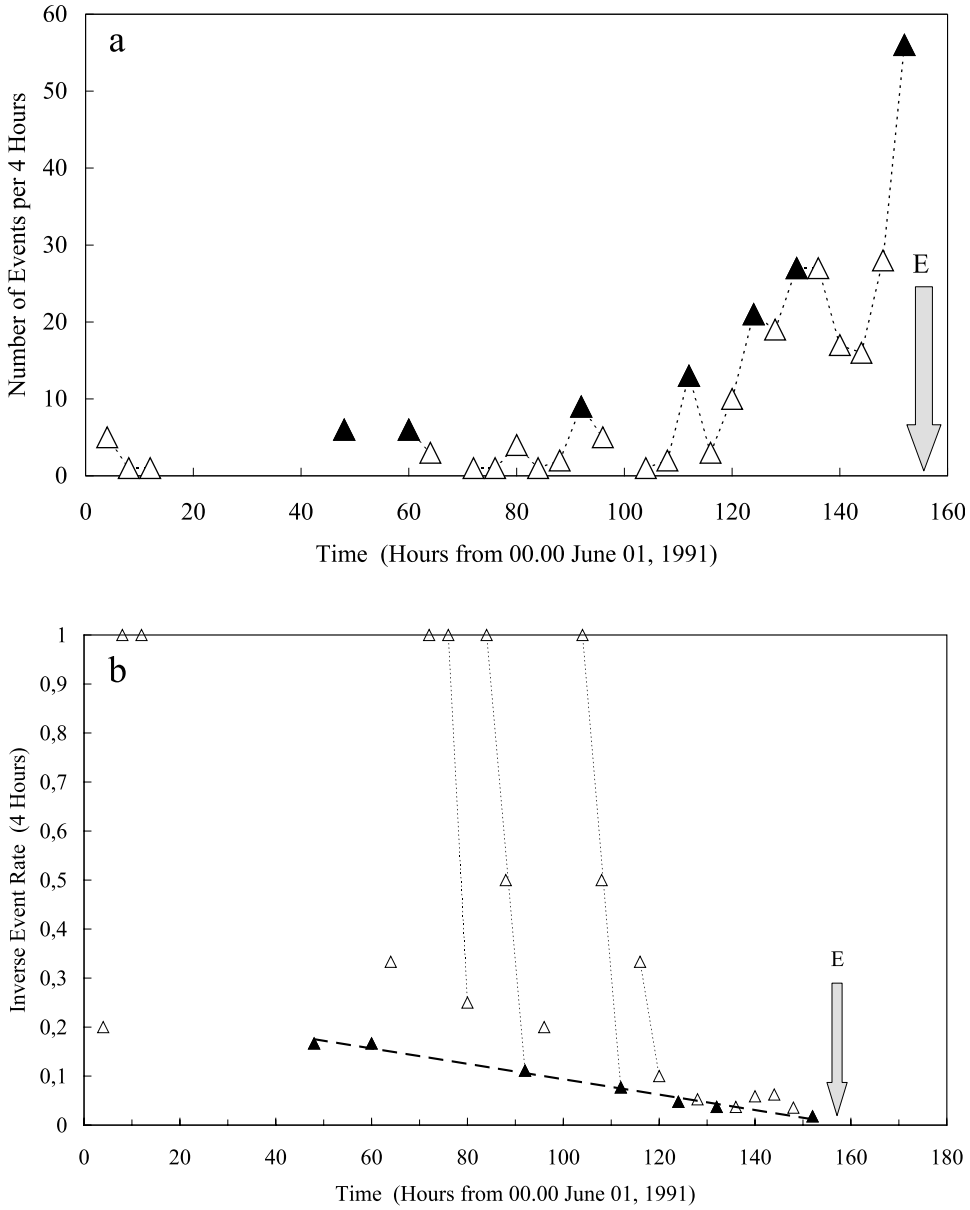

Fig. 7. (a) Change in recorded seismicity beneath the summit before the 1991 eruption of Pinatubo on Luzon in the Philippines. Filled and open triangles correspond to symbols used in panel b. Arrow E marks onset of magmatic activity. On an inverse-rate diagram (panel b), the filled triangles, which correspond to inverse-rate minima, lie along a linear trend (large dashed line). Such a trend might have been recognised by Hour 112 and so have provided a maximum 48-h warning of eruption. Note that peak values are more readily identified from the inverse-rate minima than the actual event-rate maxima, and that steeper linear trends occur among individual sequences (small dashed lines).

later than observed. By 12 November, the estimate would have been revised to 15 November. Potentially, therefore, a reliable forecast could have been made 3–6 days ahead of the eruption.

6.2. Mount Pinatubo, Luzon, Philippines, 1991

Seismic monitoring provided the primary data for evaluating the possibility of renewed activity at Mt Pinatubo in 1991, following a repose interval of some 500 years (Cornelius and Voight, 1996; Harlow et al., 1996). After magma broke the surface as a lava dome on 07 June, activity evolved to a climactic plinian eruption on 15 June. The present analysis focusses only on seismicity before the appearance of the lava dome.

Seismicity during the week before dome emplacement was characterised by an acceleration in event rate from about 10 to 60 events every 4 h (Fig. 7; Harlow et al., 1996). Between 01 and 04 June, most of the recorded earthquakes had magnitudes greater than or equal to 0.4 and were located at depths of 1–5 km about 4–5 km northwest of the volcano's summit; after 04 June, in contrast, seismicity was dominated by events with magnitudes of 1.2 or greater and located at less than about 3 km below the future summit vent (Harlow et al., 1996). The seismicity shown in Fig. 7 refers only to events recorded within the axial seismic cylinder (Harlow et al., 1996).

Harlow et al. (1996) postulated that the accelerating rate of seismicity was produced by intense brittle fracturing as magma pushed its way to the surface. Indeed, from 03 to 04 June, the 4-hourly event rate for sub-summit earthquakes shows a clear oscillation about an increasing mean trend (Fig. 7). When plotted on an inverse-rate diagram (Fig. 7), the sequence of minimum values follows a negative linear trend with time, described by:

$$(\mathrm{d}N_\mathrm{P}/\mathrm{d}t)^{-1} = 0.2515 - 0.0064t \qquad (18)$$

with an r^2 regression coefficient of 0.98 (for $\mathrm{d}N_\mathrm{P}/\mathrm{d}t$ in events per 4 h and t in units of 4 h; for t measured in hours, as in Fig. 7, Eq. 18 becomes $(\mathrm{d}N_\mathrm{P}/\mathrm{d}t)^{-1} = 0.2515 - 0.0016t$). In contrast, event-rate sequences between peaks show negative linear inverse rates with gradients of about 0.2–0.6 (estimated by eye from Fig. 7; for t in units of 4 h).

Once again, the inverse-rate trend among minimum values is consistent with that expected from the fracture-growth model. Moreover, considering only the trend that would have been apparent between 03 and 05 June (the four minima from hours 48 to 112 in Fig. 7), extrapolation of the associated regression line of $(\mathrm{d}N_\mathrm{P}/\mathrm{d}t)^{-1} = 0.2463 - 0.006t$ with $r^2 = 0.97$ (almost identical with Eq. 18) would have forecast an eruption during the evening of 07 June (hour 164), as was observed. In this case, therefore, the analysis could have provided a 48-h warning of eruption.

6.3. Implications for short-term fracture growth before eruptions

From Eqs. 14b and 15b the inverse-rate gradients for individual sequences of events and for peak event rate are, respectively, γ_2 and $\Psi\gamma_1$, where:

$$\gamma_i = B(S^2/Y')w_i\Delta c_i^2/nRT \qquad (19)$$

and the subscript i denotes the scale of cracking and all other terms are scale-independent.

For rock in compression within a volcanic edifice, $S^2/Y' \sim 10^5$ J m^{-3} (Rocchi, 2002). Temperatures may range from about 300 K at the surface to about 1200 K at the tip of the dyke; a representative value is here taken to be $T \approx 700$ K. The number n of moles in the stressed volume $V_i (= \delta_i w_i \Delta c_i)$ is $\rho\delta_i w_i \Delta c_i / W_\mathrm{m}$, where ρ and W_m are the rock's mean density and molar mass, and δ_i is the mean thickness of rock involved in releasing energy while creating the Scale-i cracks. Accordingly, Eq. 19 becomes:

$$\gamma_i = (\Delta c_i/\delta_i)[B(S^2/Y')W_\mathrm{m}/\rho RT] \qquad (20)$$

which shows that, in addition to the scale-independent terms in square brackets, the gradient for *individual* sequences depends on the geometric ratio $\Delta c_i/\delta_i$ between the step length of crack extension and the adjacent thickness of rock across which strain energy is released. It also follows from Eq. 20 that the inverse-rate gradient for peak event rates $\Psi\gamma_i = \Psi(\Delta c_i/\delta_i)B(S^2/Y')W_\mathrm{m}/\rho RT$, showing that this gradient should be smaller by a factor Ψ $(= N_i/N_{(i+1)\mathrm{P}})$ than the gradient for the individual sequences leading to each peak value.

For a fractured volcanic edifice, $\rho \approx 2200$ kg m^{-3} and $W_m \approx 0.2$ kg mol^{-1}. Hence, assuming variations about the representative values of 10% on W_m and ρ, 30% on T, and 20% on S^2/Y', and setting $B \approx \pi$, Eq. 20 yields values of: (1) γ_2 in the range $(4.5 \pm 3.2) \times 10^{-3} (\Delta c_2/\delta_2)$, and (2) the gradient among inverse peak rates in the range $(4.5 \pm 3.2) \times 10^{-3} \Psi (\Delta c_1/\delta_1)$.

To a first approximation, the thickness of rock relaxing molecular bonds (and so releasing energy) along a new crack surface is similar to the mean separation between the new surfaces of the crack (Marder and Fineberg, 1996), such that $\Delta c_1/\delta_1$ approximately describes the geometry of the c_1 crack tip via the ratio [Step length]/[Separation thickness]. From geometry, the mean separation of a Scale-i crack is also on the order of the growth step of the coalescing Scale-(i+1) cracks, such that $\delta_i \sim \Delta c_{i+1}$ (Fig. 4). Accordingly, $\Delta c_1/\delta_1 \sim \Delta c_1/\Delta c_2$.

Geometric arguments also link $\Delta c_1/\Delta c_2$ to $\Psi = N_1/N_{2P}$. Since the same growth step is being considered, the extension due to N_1 steps of length Δc_1 must be similar to N_{2P} steps of length Δc_2. Thus, $N_1 \Delta c_1 \approx N_{2P} \Delta c_2$, from which:

$$\Psi = N_1/N_{2P} \approx \Delta c_2/\Delta c_1 \approx \delta_1/\Delta c_1 \quad (21)$$

Eq. 21 shows that, because episodes of coalescence among c_2 cracks also define step advances in the larger c_1 fractures, the scaling factor Ψ is directly linked to the shape of the c_1 fracture tips, through the ratio [Separation thickness]/[Step length]. As a result, the product $\Psi(\Delta c_1/\delta_1) \approx 1$, so removing any explicit dependence on crack shape for the gradient among inverse peak rates, which simplifies from $\Psi\gamma_1$ to $\gamma^* = B(S^2/Y')W_m/\rho RT = (4.5 \pm 3.2) \times 10^{-3}$, embracing the observed values of 2.4×10^{-3} for Soufriere Hills and 6.4×10^{-3} for Pinatubo.

A key point here is that the condition $\Psi(\Delta c_1/\delta_1) \approx 1$ occurs because the growth of the main fracture system (Scale 1) is being monitored indirectly through the peak event rates of cracks at the next smaller scale (Scale 2). The same condition does not apply to individual sequences of accelerating event rate (between peak values), since the cracks being monitored are those directly responsible for the detected events (in this case, all at Scale 2). Indeed, for each precursory sequence, the ratio of the gradient for an inverse-rate sequence to the gradient among inverse peak rates is $\gamma_2/\Psi\gamma_1 = (1/\Psi)(\Delta c_2/\Delta c_3)(\Delta c_2/\Delta c_1) \approx 1/\Psi$, assuming that the difference in mean crack dimensions remains the same among any pair of successive length scales. From Figs. 6 and 7, $1/\Psi = 0.01/0.0024 \approx 4$ for Soufriere Hills and about (0.2 to 0.6)/0.0064 $\approx$ 30 to 90 (notionally 60) for Pinatubo. Compared with conditions at Soufriere Hills, therefore, each growth step of the main Pinatubo fracture apparently required the coalescence of a greater number, by a factor of about 15, of smaller process-zone cracks. In other words, the tips of fractures extending beneath Pinatubo may have been about 15 times more elongate with respect to those extending beneath Soufriere Hills.

7. Discussion

A remarkable feature of the inverse-rate trends for seismic precursors at Soufriere Hills and Pinatubo is that, although the gradients for individual sequences differ by more than an order of magnitude, the gradients for inverse peak values are within a factor of three of each other (Eqs. 17 and 18). Such a coincidence suggests a common controlling mechanism. Thus, combining Eqs. 20 and 21 with Eq. 15a,b yields for the trends among peak rates dN_P/dt:

$$dN_P/dt = \beta e^{\gamma^* N_P} \quad (22a)$$

$$(dN_P/dt)^{-1} = (dN_P/dt)_0^{-1} - \gamma^*(t - t_0) \quad (22b)$$

where $\gamma^* = B(S^2/Y')W_m/\rho RT$ and β is a constant containing the remaining energy terms; γ^* is the ratio [Strain energy per unit volume]/[Total internal energy per unit volume], but can also be viewed as $1/N^*$ where N^* is the effective number of seismic events required to release the total internal energy as strain energy (if such a complete conversion were possible). The linear dependence of inverse peak rate with time (Eq. 22b) is especially favourable to forecasting since it requires only the extrapolation of a straight line to the time axis in order to identify a possible time of

eruption. Moreover, the inverse peak values (minima on the inverse-rate plot) may be easier to identify by eye than the actual peak values (on the event-rate plot) under emergency conditions (compare, for example, Fig. 6a,b).

Applied to the observed precursors (Figs. 6 and 7), the measured values of γ^* are within the range of $(4.5 \pm 3.2) \times 10^{-3}$ expected for conditions within a subvolcanic system. Such agreement is excellent and not only supports the validity of the slow-fracture model, but also suggests that reliable forecasts of eruption might eventually be feasible at least 2–3 days ahead of time. Warning intervals of days are relevant in practice because they may permit successful evacuation of threatened districts.

The restricted range for γ^* is another feature with possible forecasting implications. It is a natural consequence of using peak rates of process-zone cracking as a proxy measure for growth steps among the parent fractures, since this substitution cancels terms that depend on crack-tip geometry. Seismic monitoring systems, however, are deployed to detect as many events as possible. It is thus by happy circumstance, rather than by design, that the majority of detected events appear to be those relevant to cracking in the process zones of the dominant existing fractures. Detected events commonly have magnitudes of about 0–2, consistent with movements of 1–10 mm over 10–100 m (McNutt, 2000). The fact that a negative gradient of γ^* (rather than a steeper gradient) is found for their inverse-peak-rate trend therefore suggests that the detected events relate either (a) to movements in the process zones of primary fractures that are typically several tens of metres long, such that each event reflects slip along a primary fracture, or (b) to movements of fractures tens of metres long that form part of the process zones of primary fractures (perhaps $\sim 10^2$ m long), in which case slip along the parent fractures is detected as a swarm of small events, rather than a small number of events of larger magnitude. Whatever the interpretation, if such a condition exists among volcanoes in general, it follows that the opening of a new magmatic pathway will be characterised by inverse-peak-rate trends with gradients of γ^*, as opposed to the steeper gradients that characterise the inverse-rate trends of individual process-zone sequences (Fig. 5). An inverse-rate gradient of γ^* might thus also be indicative of the final approach to eruption.

The present model has been tested against only two examples, both of them related to andesitic volcanoes reawakening after centuries of quiescence. However, because it focusses on the fracture behaviour of host rock (in response to stresses applied due to increased magma pressure), there is no immediately obvious reason why it should not apply generally to conditions in which the opening of a new magmatic pathway is essential for an eruption to occur. It may thus be found useful, for example, also for describing the lateral propagation of fractures from the central feeding system of persistently active basaltic volcanoes, such as Etna or Stromboli. On the other hand, it would be less useful for describing seismic precursors to eruptions from vents that are already open, corresponding to conditions that may apply, for example, (a) to summit effusions at persistently active volcanoes, and (b) to subsequent eruptive episodes through a pathway that had been created only shortly beforehand during the reawakening of a long-quiescent volcano.

The present model further introduces the notion of describing an opening magmatic pathway in terms of the progressive linkage of a population of existing fractures. This notion accommodates the observation that the locations of seismic precursors do not always migrate towards the surface with time. It also provides the basis for treating macroscopic seismic event rates statistically through random fluctuations in the release of stress-related energy, an approach which naturally explains the similar types of acceleration in event rate with time observed for both microscopic and macroscopic fracturing.

However, although the model describes the growth of a major fracture system, it cannot guarantee that the new fracture will intersect both a magma body and the surface. Thus, if only the magma body is intersected, the result may be an upward intrusion, rather than eruption. Similarly, if the magma body is not reached, displacement along the new fracture may instead trigger an

earthquake or an intense seismic swarm. Thus, although eruptions may be preceded by seismic sequences similar to those analysed here, it is not evident that all such sequences inevitably lead to eruption. They may instead be followed by a permanent decay in activity or by a temporary lull in seismicity (McNutt, 1996). To guarantee an eruption, therefore, additional criteria must also be satisfied. Such criteria may be deterministic (e.g. the volcanic edifice may first have to be stretched by a critical amount) or stochastic (e.g. whether or not a fracture intersects a magma body may contain an element of chance, perhaps due to edifice heterogeneity). In either case, the present analysis provides a basis on which new studies can build for identifying the additional pre-eruption requirements.

The present model also assumes that, in the final approach to eruption, detected seismicity is dominated by events driven by magmatic pressure applied axially below the future eruptive vent. It does not account (a) for seismicity induced by factors other than magma pressure, such as thermal cracking, or (b) for detected events due to fracturing at locations away from the axial seismic cylinder. Future analyses may be able to filter out signals produced by non-magmatic stresses, while the eventual real-time location of events would distinguish fracturing within and outside the axial seismic cylinder.

The slow-fracture model is a natural extension of the pioneering studies by Voight (1988, 1989) and their development by Voight and Cornelius (1991) and Cornelius and Voight (1994, 1995, 1996). Unlike the present model, which focusses on changes in peak seismic event rate, the previous studies concentrated on changes in mean event rate. The Voight and Cornelius studies also suggested that, in addition to linear decreases with time, inverse rates may on occasion decay exponentially with time (corresponding to the condition $\alpha = 1$ in Eq. 1). Such decay would approach a zero inverse rate (time of eruption) after an unspecified interval and so cannot be used for eruption forecasting, unless independent arguments can also identify a non-zero threshold rate of seismicity at which an eruption is expected. This behaviour has been attributed to the growth of cracks that do not eventually coalesce and so do not lead to the opening of a new magmatic pathway (McGuire and Kilburn, 1997; Kilburn and Voight, 1998); as discussed above, contributors to such cracking may include non-magmatic stresses and events occurring outside the axial seismic cylinder. However, such behaviour might also represent a condition for which a rate-dependent resistance, perhaps along moving faults (Dieterich, 1992), becomes large enough to inhibit further slow fracture. Thus, a more complete form of Eq. 22a may be:

$$\mathrm{d}N_P/\mathrm{d}t = \beta \mathrm{e}^{\gamma^* N_P} - f(R) \quad (23)$$

where the resisting term $f(R)$ is small for conditions that finally result in eruption. The significance of such a resisting term awaits future study.

8. Conclusions

The present model argues that the final stages of magma ascent are controlled by the slow fracturing of host rock between a magma body and the surface. Fracturing occurs by the growth and coalescence of pre-existing cracks. Each crack itself has a process zone containing even smaller cracks. Failure is thus perceived as a multiscale process for which microscopic cracking can ultimately lead to macroscopic fracturing. Since similar processes are assumed to operate at all scales, the form of the governing crack-growth equation remains the same, independent of the size and duration of cracking being investigated. Similar seismic patterns are therefore anticipated among eruption precursors, irrespective of the time scale used to measure event rate. Indeed, the examples from Soufriere Hills and Pinatubo (Figs. 6 and 7) illustrate how the same essential pattern emerges for event rates measured, respectively, every 4 h and per day, and suggest that reliable forecasts of eruption might be feasible at least 2–3 days ahead of time. Further studies, however, are required to confirm the present results and, also, to identify the broader range of conditions that distinguish accelerations in seismic event rate that may decay without volcanic activity from those that will inevitably lead to eruption.

Acknowledgements

This paper benefitted from discussions with Peter Sammonds and Valentina Rocchi (both at UCL) and from helpful reviews by Sebastien Chastin (University of Edinburgh) and Steve McNutt (Alaska Volcano Observatory). The research was funded by the European Commission (DG Research, Environment and Climate programme, Natural Risks, A. Ghazi, Head of Unit, Maria Yeroyanni, Scientific Officer) for Project Volcalert (CEC Contract No. EVG-2001-00040) and by the Gruppo Nazionale per la Vulcanologia, Italy.

Appendix. Manipulation of the event-rate equation

From Eq. 12 in the main text:

$$\mathrm{d}N/\mathrm{d}t = C\mathrm{e}^{\gamma N} \tag{A1}$$

where the constant $C = f^{*}\mathrm{e}^{-\eta}\mathrm{e}^{\gamma c_0/\Delta c}$.

Rearrangement of Eq. A1 leads to:

$$\int_{N_0}^{N} \exp(-\gamma N)\mathrm{d}N = C\int_{t_0}^{t}\mathrm{d}t \tag{A2}$$

which yields:

$$(\mathrm{e}^{-\gamma N_0}/C) - (\mathrm{e}^{-\gamma N}/C) = \gamma(t - t_0) \tag{A3}$$

Noting from Eq. A1 that $(\mathrm{d}N/\mathrm{d}t)^{-1} = \mathrm{e}^{-\gamma N}/C$, Eq. A3 becomes:

$$(\mathrm{d}N/\mathrm{d}t)^{-1} = (\mathrm{d}N/\mathrm{d}t)_0^{-1} - \gamma(t - t_0) \tag{A4}$$

where $(\mathrm{d}N/\mathrm{d}t)_0$ is the value of $\mathrm{d}N/\mathrm{d}t$ at $t = t_0$, identical with Eq. 13 in the main text.

The values of t_0 and, hence, of $(\mathrm{d}N/\mathrm{d}t)_0$ are normally determined empirically from graphs of accelerating event rate. However, $(\mathrm{d}N/\mathrm{d}t)_0$ can in principle also be calculated from Eq. A1 as $f^{*}\mathrm{e}^{-\eta}\mathrm{e}^{\gamma c_i/\Delta c}\mathrm{e}^{\gamma N_0}$ or, using Eq. 11, as $f^{*}\mathrm{e}^{-\varepsilon_{i0}/nRT}$ where ε_{i0} is the excess energy required to start the acceleration in rate of rock fracturing.

References

Anderson, O.L., Grew, P.C., 1977. Stress corrosion theory of crack propagation with applications to geophysics. Rev. Geophys. Space Sci. 15, 77–104.

Aspinall, W.P., Miller, A.D., Lynch, L.L., Latchman, J.L., Stewart, R.C., White, R.A., Power, J.A., 1998. Soufrière Hills eruption, Montserrat, 1995-1997: Volcanic earthquake locations and fault plane solutions. J. Geophys. Res. 25, 3397–3400.

Atkinson, B.K., 1984. Subcritical crack growth in geological materials. J. Geophys. Res. 89, 4077–4114.

Charles, R.J., Hillig, W.B., 1962. The kinetics of glass failure by stress corrosion. In: Symposium sur la resistance mechanique du verre et les moyens de l'ameliorer. Union Sciences Continentale du Verre, Charleroi, 511 pp.

Chouet, B.A., 1996. New methods and future trends in seismological volcano monitoring. In: Scarpa, R., Tilling, R.I. (Eds.), Monitoring and Mitigation of Volcano Hazards. Springer, Berlin, pp. 23–97.

Cornelius, R.R., Voight, B., 1994. Seismological aspects of the 1989-1990 eruption at Redoubt volcano, Alaska: the materials failure forecast method (FFM) with RSAM and SSAM seismic data. J. Volcanol. Geotherm. Res. 62, 469–498.

Cornelius, R.R., Voight, B., 1995. Graphical and PC-software analysis of volcano eruption precursors according to the Materials Failure Forecast Method (FFM). J. Volcanol. Geotherm. Res. 64, 295–320.

Cornelius, R.R., Voight, B., 1996. Real-time seismic amplitude measurement (RSAM) and seismic spectral amplitude measurement (SSAM) analyses with the Materials Failure Forecast Method (FFM), June 1991 explosive eruption at Mount Pinatubo. In: Newhall, C.G., Punongbayan, R.S. (Eds.), Fire and Mud: Eruptions and Lahars of Mount Pinatubo, Philippines. PHIVOLCS, Quezon City, and University of Washington Press, Seattle, WA, pp. 249–267.

Cowie, P.A., 1998. A healing-reloading feedback control on the growth rate of seismogenic faults. J. Struct. Geol. 20, 1075–1087.

Cowie, P.A., Shipton, Z.K., 1998. Fault tip displacement gradients and process zone dimensions. J. Struct. Geol. 20, 983–997.

De la Cruz-Reyna, S., Reyes-Dávila, G.A., 2001. A model to describe precursory material-failure phenomena: applications to short-term forecasting at Colima volcano, Mexico. Bull. Volcanol. 63, 297–308.

De Natale, G., Pingue, F., Allard, P., Zollo, A., 1991. Geophysical and geochemical modeling of the 1982-1984 unrest phenomena at Campi Flegrei caldera (Southern Italy). J. Volcanol. Geotherm. Res. 48, 199–222.

Dieterich, J.H., 1992. Earthquake nucleation on faults with rate- and state-dependent strength. Tectonophysics 211, 115–134.

Griffith, A.A., 1920. The phenomenon of rupture and flow in solids. Philos. Trans. R. Soc. London A 221, 163–197.

Harlow, D.H., Power, J.A., Laguerta, E.P., Ambubuyong, G., White, R.A., Hoblitt, R.P., 1996. Precursory seismicity and forecasting of the June 15, 1991, eruption of Mount Pinatubo. In: Newhall, C.G., Punongbayan, R.S. (Eds.), Fire and Mud: Eruptions and Lahars of Mount Pinatubo, Philip-

pines. PHIVOLCS, Quezon City, and University of Washington Press, Seattle, WA, pp. 285–305.
Heimpel, M., Olson, P., 1994. Buoyancy-driven fracture and magma transport through the lithosphere: models and experiments. In: Ryan, M.P. (Ed.), Magmatic Systems. Academic Press, San Diego, CA, pp. 223–240.
Hill, D.P., Ellsworth, W.L., Johnston, M.J.S., Langbein, J.O., Oppenheimer, D.H., Pitt, A.M., Reasenburg, P.A., Sorey, M.L., McNutt, S.R., 1990. The 1989 earthquake swarm beneath Mammoth Mountain, California: an initial look at the 4 May through 30 September activity. Bull. Seism. Soc. Am. 80, 325–339.
Jaeger, J.C., 1969. Elasticity, Fracture and Flow, 3rd edn. Chapman and Hall, London, 268 pp.
Kilburn, C.R.J., Voight, B., 1998. Slow rock fracture as eruption precursor at Soufriere Hills volcano, Montserrat. Geophys. Res. Lett. 25, 3665–3668.
Landau, L.D., Lifshitz, E.M., 1999. Statistical Physics, Part 1, 3rd edn. Butterfield Heinemann, 546 pp.
Lawn, B., 1993. Fracture of Brittle Solids, 2nd edn. Cambridge University Press, Cambridge, 378 pp.
Lister, J.R., 1991. Steady solutions for feeder dykes in a density-stratified lithosphere. Earth Planet. Sci. Lett. 107, 233–242.
Lockner, D., 1993. Room temperature creep in saturated granite. J. Geophys. Res. 98, 475–487.
Main, I.G., 1991. A modified Griffith criterion for the evolution of damage with a fractal distribution of crack lengths: application to seismic event rates and *b*-values. Geophys. J. Int. 107, 353–362.
Main, I.G., Meredith, P.G., 1991. Stress corrosion constitutive laws as a possible mechanism of intermediate-term and short-term seismic event rates and *b*-values. Geophys. J. Int. 107, 363–372.
Main, I.G., 1999. Applicability of time-to-failure analysis to accelerated strain before earthquakes and volcanic eruptions. Geophys. J. Int. 139, F1–F6.
Main, I.G., 2000. A damage mechanics model for power-law creep and earthquake aftershock and foreshock sequences. Geophys. J. Int. 142, 151–161.
Marder, M. Fineberg, J., 1996. How things break. Physics Today (September) 24–29.
McGuire, W.J., Kilburn, C.R.J., 1997. Forecasting volcanic events: some contemporary issues. Geol. Rundsch. 86, 439–445.
McGuire, W.J., Kilburn, C.R.J., Murray, J.B. (Eds.), 1995. Monitoring Active Volcanoes: Strategies, Procedures and Techniques. UCL Press, London, 421 pp.
McNutt, S.R., 1996. Seismic monitoring and eruption forecasting of volcanoes: a review of the state-of-the-art and case histories. In: Scarpa, R., Tilling, R.I. (Eds.), Monitoring and Mitigation of Volcano Hazards. Springer, Berlin, pp. 99–146.
McNutt, S.R., 2000. Volcano seismicity. In: Sigurdsson, H. (Ed.), Encyclopedia of Volcanoes. Academic Press, San Diego, CA, pp. 1015–1033.
Newhall, C.G., Punongbayan, R.S. (Eds.), 1996. Fire and Mud: Eruptions and Lahars of Mount Pinatubo, Philippines. PHIVOLCS, Quezon City, and University of Washington Press, Seattle, WA.
Power, J.A., Wyss, M., Latchman, J.L., 1998. Spatial variations in the frequency-magnitude distribution of earthquakes at Soufriere Hills Volcano, Montserrat, West Indies. Geophys. Res. Lett. 25, 3653–3656.
Reyes-Dávila, G.A., De la Cruz-Reyna, S., 2002. Experience in the short-term eruption forecasting at Volcán de Colima, México, and public response to forecasts. J. Volcanol. Geotherm. Res. 117, 121–127.
Rocchi, V., 2002. Fracture of basalts under simulated volcanic conditions. Ph.D. thesis, University of London, 390 pp.
Ruhla, C., 1992. The Physics of Chance. Oxford University Press, Oxford, 222 pp.
Savage, J.C., Cockerham, R.S., 1984. Earthquake swarm in Long Valley caldera, California, January 1983: evidence for dike injection. J. Geophys. Res. 89, 8315–8324.
Scarpa, R., Tilling, R.I. (Eds.), 1996. Monitoring and Mitigation of Volcano Hazards. Springer, Berlin, 841 pp.
Scholz, C.H., 1990. The Mechanics of Earthquakes and Faulting. Cambridge University Press, Cambridge, 439 pp.
Shaw, H.R., 1980. The fracture mechanisms of magma transport from the mantle to the surface. In: Hargraves, R.B. (Ed.), Physics of Magmatic Processes. Princeton University Press, Princeton, NJ, pp. 201–264.
Sigurdsson, H. (Ed.), 2000. Encyclopedia of Volcanoes. Academic Press, San Diego, CA, 1417 pp.
Smith, G.M., Ryall, F.D., 1982. Bulletin of the Seismological Laboratory for the period January 1 to December 13, 1980. Mackay School of Mines, University of Nevada, Reno, NV, 50 pp.
Spence, D.A., Turcotte, D.L., 1985. Magma-driven propagation of cracks. J. Geophys. Res. 90, 575–580.
Voight, B., 1988. A method for prediction of volcanic eruptions. Nature 332, 125–130.
Voight, B., 1989. A relation to describe rate-dependent material failure. Science 243, 200–203.
Voight, B., Cornelius, R.R., 1991. Prospects for eruption prediction in near real-time. Nature 350, 695–698.
Wiederhorn, S.M., Bolz, L.H., 1970. Stress corrosion and static fatigue of glass. J. Am. Ceram. Soc. 53, 543–548.
Young, S.R., Sparks, R.S.J., Aspinall, W.P., Lynch, L.L., Miller, A.D., Robertson, R.E.A., Shepherd, J.B., 1998. Overview of the eruption of Soufriere Hills volcano, Montserrat, 18 July 1995 to December 1997. Geophys. Res. Lett. 25, 3389–3392.